analytical chemistry

pubs.acs.org/ac Article

Boron Carbon Nitride Nanosheets-Ru Nanocomposite Self-Enhancement Electrochemiluminescence Emitter with a Three-Dimensional DNA Network Structure as a Signal Amplifier for Ultrasensitive Detection of TK1 mRNA

Jicui Hu, Yue Zhang, Yaqin Chai,* and Ruo Yuan*

Cite This: *Anal. Chem.* 2022, 94, 11345−11351 Read Online

ACCESS | Metrics & More | Article Recommendations | Supporting Information

ABSTRACT: In this study, a neoteric self-enhanced nanocomposite boron carbon nitride nanosheets (BCN NSs)-Ru obtained by chemical crosslinking between boron carbon nitride nanosheets (BCN NSs) and tris (4,4′-dicarboxylicacid-2,2′-bipyridyl) ruthenium(II) dichloride ($Ru(dcbpy)_3Cl_2$) was used as an emitter to build an electrochemiluminescence (ECL) biosensor for ultrasensitive detection of the cancer marker human thymidine kinase 1 (TK1) mRNA. Importantly, the self-enhanced BCN NSs-Ru could exhibit strong ECL emission because boron radicals and amine groups derived from BCN NSs could significantly enhance the ECL response of $Ru(dcbpy)_3Cl_2$, which avoided the defects of the long electron transfer path and large energy loss between the emitter and coreactant in the traditional coreaction ECL system. Impressively, in the presence of target TK1 mRNA, three-dimensional DNA network structure-labeled numerous ferrocene probes could be assembled to quickly quench the ECL signal of BCN NSs-Ru, resulting in improved biosensor sensitivity. The obtained "on−off" biosensor showed excellent stability and high sensitivity with a detection limit of 32.3 aM. In general, the developed strategy provided a new biosensing way for ultrasensitive detection of biomolecules in early disease diagnosis.

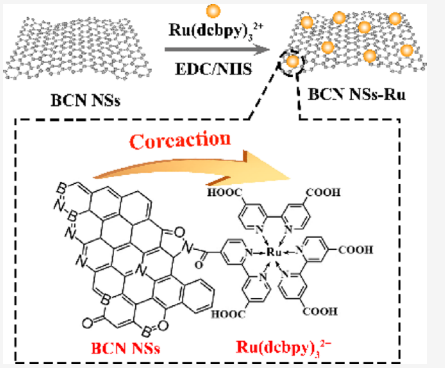

INTRODUCTION

Electrochemiluminescence (ECL), a form of energy relaxation, was triggered by the electrochemical stimulation, which was attracting increasing interest in a variety of areas,[1−3] such as clinical diagnosis, environmental regulation, food analysis, and drug detection on account of low background, high sensitivity, and excellent controllability.[4−7] In the coreactant ECL system, the coreactant was indispensable to improve the ECL efficiency of the emitter.[8−12] However, the reaction between the external coreactant and emitter in the traditional coreactant ECL system had certain disadvantages of slow electron transfer speed and low ECL efficiency, limiting the improvement of ECL strength.[13,14] Therefore, it was particularly important to explore an efficient ECL emitter to avoid the electron transmission obstruction and large energy loss between the emitter and coreactant in solution. On account of the $\pi-\pi$ stacking and electrostatic interactions as well as the stimulation of electrical activity by heteropolar B−N bonding, boron carbon nitride nanosheets (BCN NSs) exhibited striking performance such as extraordinary chemical stability, excellent adsorption, and impressive oxygen reduction reaction catalysis.[15−17] Moreover, the electronic tunneling among the ultrathin BCN NSs' interlamination could realize faster electron transfer, which was conducive to the rapid and effective intramolecular reaction. Impressively, the amine groups and the unsaturated boron atom at the edges or defects of BCN NSs, which were a source of active radicals, could be used as the ECL coreactant of tris (4,4′-dicarboxylicacid-2,2′-bipyridyl) ruthenium(II) ($Ru(dcbpy)_3^{2+}$).[18,19] In this work, BCN NSs as a novel coreactant were covalently combined with $Ru(dcbpy)_3^{2+}$ to synthesize a self-enhanced ECL emitter BCN NSs-Ru with amazing ECL efficiency in the absence of any additional coreactants, which would create a new path to synthesize self-enhanced ECL emitters with superior performance.

Messenger RNA (mRNA) played an important role in the synthesis of proteins, which was also an effective cancer biomarker.[20−25] For instance, human thymidine kinase 1 (TK1) mRNA was associated with the activity of cell cycle regulatory enzyme TK1, and TK1 was involved in cell proliferation.[26,27] Thus, TK1 mRNA had been used as a

Received: May 15, 2022
Accepted: July 25, 2022
Published: August 2, 2022

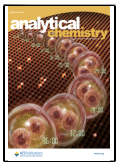

https://doi.org/10.1021/acs.analchem.2c02110
Anal. Chem. 2022, 94, 11345−11351

Scheme 1. Assembly Process of DNA Nanoflowers DNF 1 and DNF 2 (A), Preparation of BCN NSs-Ru (B), and Construction of the TK1 mRNA Biosensor and the Response Signal (C)

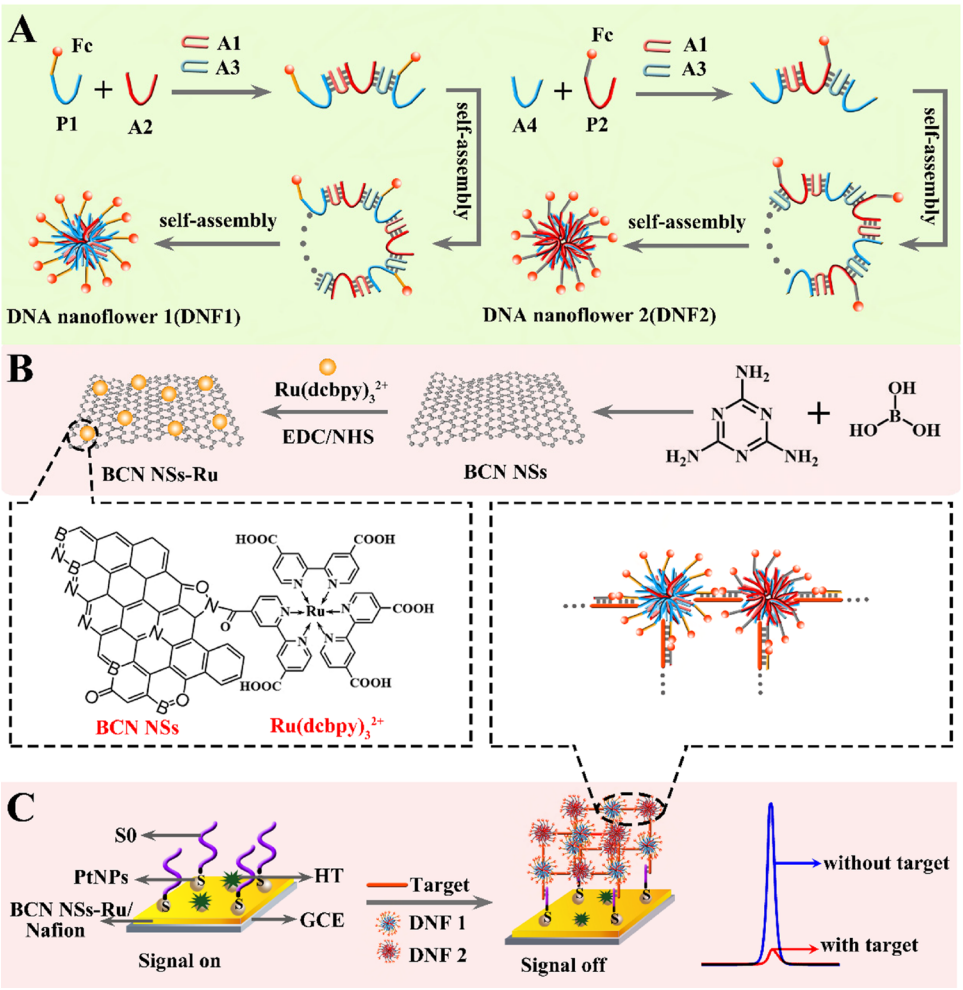

specific indicator of cancer to reflect the development of the disease. Currently, various methods had been reported to identify and detect mRNA, such as fluorescence in situ hybridization, electrochemical analysis, and protein labeling methods.[28−30] However, these methods with low sensitivity cannot be used for the detection of trace biomarkers. Therefore, for the precise detection of specific mRNA, new target amplification strategies were urgently required.[31−33] At present, to enhance the sensitivity of target detection, various DNA structures, such as DNA dendrimers,[17−20] four-way DNA junctions,[21−24] and three-dimensional (3D) DNA matrices,[34] have been designed to immobilize massive signal probes. However, these DNA structures had the disadvantages of finite rigidity, complex synthesis, and limited attached probes, which hindered the further improvement of biosensor sensitivity.[34−36] Herein, two similar DNA nanoflowers (labeled DNF 1 and DNF 2) were self-assembled from four kinds of DNAs to assemble a target-induced 3D DNA network structure for immobilization of numerous quenchers used for significant signal amplification. Moreover, the novel approach proved that the network could serve as an efficient ECL signal converter and paved the way for the application of the target amplification strategy in biosensors.

In this work, based on the novel self-enhanced BCN NSs-Ru as an ECL emitter and target-induced 3D DNA network structure as a signal converter, the ultrasensitive ECL biosensor was fabricated for the detection of human thymidine kinase 1 (TK1) mRNA, which has been used as a specific indicator of tumor growth to reflect the development of the disease. Initially, Scheme 1A was the assembly diagram of DNF 1 and DNF 2 with a large number of ferrocene-modified probes obtained through the Watson−Crick base pairing principle. Meanwhile, the BCN NSs were synthesized by directly heating a mixture of boric acid and melamine, which was further covalently associated with $Ru(dcbpy)_3Cl_2$ to form the self-enhanced nanocomposite BCN NSs-Ru (Scheme 1B). In Scheme 1C, a mixture of BCN NSs-Ru, Pt NPs, and Nafion was first covered on the surface of the glassy carbon electrode (GCE) to offer a strong ECL initialized signal (signal on). Next, the DNA probe S0 labeled with sulfhydryl was attached to the BCN NSs-Ru/Pt NPs/Nafion. Afterward, the 3D network structure was successfully constructed on the electrode surface via the hybridization chain reaction of DNF 1 and DNF 2 with a lot of ferrocene triggered by target TK1 mRNA to significantly quench the strong ECL signal (signal off), achieving ultrasensitive detection of the aM level of TK1 mRNA. This strategy provided a new idea for the application of the self-enhanced ECL emitter in biomolecular detection and disease diagnosis.

https://doi.org/10.1021/acs.analchem.2c02110
Anal. Chem. 2022, 94, 11345−11351

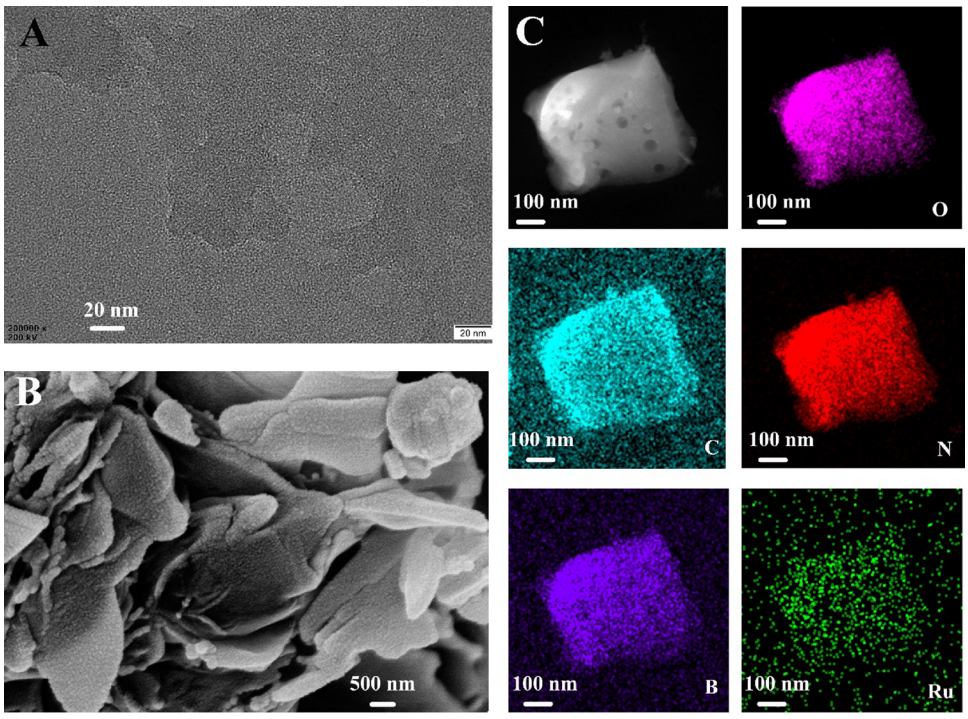

Figure 1. TEM (A) and SEM (B) images of the BCN NSs; scanning TEM image (C) and corresponding EDS elemental (O, C, N, B, and Ru) mapping for BCN NSs-Ru.

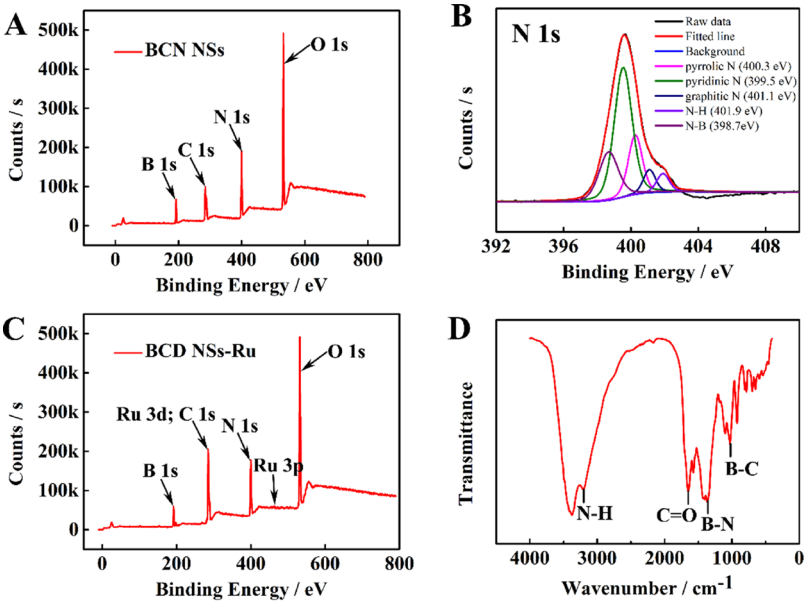

Figure 2. XPS spectra of BCN NSs (A) and high-resolution N 1s spectrum (B). XPS (C) and FTIR (D) spectra of BCN NSs-Ru.

EXPERIMENTAL SECTION

Reagents and Apparatus. A detailed description of reagents and apparatus used in this work is shown in the Supporting Information.

Fabrication of the Developed ECL Biosensor. First, 10 μL of the mixture BCN NSs-Ru/Pt nanoparticles (Pt NPs)/Nafion was dripped on the surface of the preprocessed GCE (Φ = 4 mm), drying at 37 °C naturally. Later, 10 μL of 2 μM S0 was attached to the surface of the modified GCE by incubating overnight at 4 °C. Then, 10 μL of 1 mM 1-hexanethiol (HT) was incubated on the GCE for 40 min, so the remaining binding sites of Pt NPs could be blocked. After mixing the three solutions of DNF 1 and DNF 2 and various concentrations of TK1 mRNA, 10 μL of the above mixture was dripped onto the above-modified electrode and incubated for 120 min at 37 °C to construct the biosensor.

Measurement Procedure of ECL and Electrochemical Analysis. The proposed ECL biosensor was tested in 2 mL of PBS (0.10 M, pH 7.4) to record the ECL signal. The potential scanning ranged from +0.2 ~ +1.25 V with the voltage of the photomultiplier tube at 800 V and a scan rate of 0.3 V s^{-1}. The cyclic voltammograms were recorded in 5.0 mM $[Fe(CN)_6]^{3-/4-}$ from −0.2 to +0.6 V at a scan rate of 0.1 V s^{-1}.

https://doi.org/10.1021/acs.analchem.2c02110
Anal. Chem. 2022, 94, 11345−11351

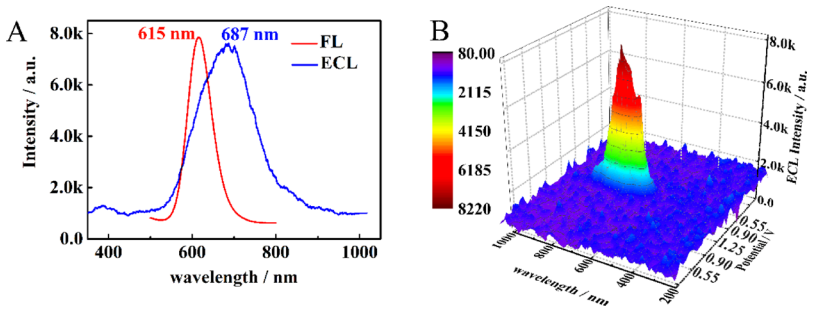

Figure 3. (A) FL and ECL spectrum of BCN NSs-Ru; (B) 3D ECL surface image of BCN NSs-Ru.

RESULTS AND DISCUSSION

Characterization of the BCN NSs and BCN NSs-Ru. Transmission electron microscopy (TEM), scanning electron microscopy (SEM), and atomic force microscopy (AFM) were implemented to study the morphology of BCN NSs. In Figure 1A,B, the BCN NSs were irregularly flaky and accumulated from multiple layers. In addition, the AFM analysis showed that the height of the BCN NSs was 2.5 ± 0.5 nm (Figure S2A,B), which illustrated the successful synthesis of the BCN NSs. Then, the element distribution of the BCN NSs-Ru was revealed by energy-dispersive X-ray spectroscopy (EDS) (Figure 1C), and some elements containing O, C, N, B, and Ru were homogeneously distributed in the BCN NSs-Ru, confirming that $Ru(dcbpy)_3^{2+}$ was successfully doped into the BCN NSs-Ru.

Additionally, X-ray photoelectron spectroscopy (XPS) and Fourier transform infrared (FTIR) analyses were carried out to further certify the successful preparation of the BCN NSs-Ru. As seen in Figure 2A, the XPS characteristic peaks of B 1s, O 1s, N 1s, and C 1s were presented at 205, 545, 410, and 298 eV, respectively. In addition, the high-resolution N 1s spectrum belonging to BCN NSs (Figure 2B) possessed five typical fitted peaks at 400.3 eV (pyrrolic N), 399.5 eV (pyridinic N), 401.1 eV (graphitic N), 401.9 eV (N−H), and 398.7 eV (N−B). After the covalent bonding of $Ru(dcbpy)_3^{2+}$ into BCN NSs, the XPS characteristic peaks of Ru 3p and Ru 3d were recorded at 496 and 285 eV (Figure 2C), respectively, which certified the presence of $Ru(dcbpy)_3^{2+}$ in the nanocomposite. As demonstrated in Figure 2D, BCN NSs-Ru displayed characteristic peaks generated by the N−H and C═O stretching at 3207 and 1650 cm^{-1}, respectively, illustrating the formation of amide bonds in BCN NSS-Ru. Beyond that, the peaks at 1366 and 1028 cm^{-1} originated from the B−N stretching and the cubical B−C vibrations.

Fluorescence (FL) and ECL Spectral Analysis of BCN NSs-Ru. The FL and ECL spectra were recorded to research the luminescence properties of composite BCN NSs-Ru. In Figure 3A, the FL emission peak of BCN NSs-Ru was at 615 nm, and the ECL emission peak was at 687 nm, which showed a red shift of 72 nm in the ECL spectrum compared with the FL emission due to an inner-filter effect. In addition, Figure 3B shows the maximum ECL emission wavelength at 687 nm in the scanning potential range of +0.2 ∼ +1.25 V.

Self-Enhanced Mechanism of BCN NSs-Ru. According to the literature,[4,13,18,19,37] taking the amine oxidation mechanism of BCN NSs as an example, the possible ECL self-enhanced mechanism of BCN NSS-Ru was as follows (eqs 1234). With positive potential scanning, the components of BCN NSS-Ru(II) were oxidized to form BCN NSS-$Ru(III)^{\bullet+}$ (eq 1), which was further deprotonated to form a BCN NSS-$Ru(III)^{\bullet}$ intermediate (eq 2). Then, the strongly oxidized intermediate was transformed into an excited state BCN NSS-Ru(II)*, which could return to the ground state accompanied by strong ECL emission via intramolecular electron and energy transfer (eq 4).

$$\text{BCN NSs} - \text{Ru}_{(\text{II})} - 2e^- \rightarrow \text{BCN NSs} - \text{Ru}_{(\text{III})}^{\bullet+} \quad (1)$$

$$\text{BCN NSs} - \text{Ru}_{(\text{III})}^{\bullet+} \rightarrow \text{BCN NSs} - \text{Ru}_{(\text{III})}^{\bullet} + \text{H}^+ \quad (2)$$

$$\text{BCN NSs} - \text{Ru}_{(\text{III})}^{\bullet} \rightarrow \text{BCN NSs} - \text{Ru}_{(\text{II})}^{*} + \text{H}^+ \quad (3)$$

$$\text{BCN NSs} - \text{Ru}_{(\text{II})}^{*} \rightarrow \text{BCN NSs} - \text{Ru} + h\nu \quad (4)$$

Characterization of the DNA Reaction. Polyacrylamide gel electrophoresis (PAGE) was applied to explore the feasibility of the DNA reaction. In Figure 4A, seven single strands of DNA (A1, A2, A3, A4, P1, P2, TK1 mRNA) emerged as bright bands (lane 1−7) at different locations separately. In addition, the clear band at the top of lane 8 and lane 9 indicated that DNF 1 and DNF 2 were successfully self-assembled. In addition, TEM and AFM also were used for morphology characterization of DNF (Figure S3). In the presence of target TK1 mRNA, the two kinds of DNF were assembled into the 3D DNA network structure to form lane 10, demonstrating that the TK1 mRNA could drive the construction of the DNA network structure. When DNF 1, DNF 2, TK1 mRNA, and S0 were mixed for incubation, the band of S0 almost disappeared and a clear band at the top of lane 5 (in Figure 4B) arose, indicating that S0 hybridized with the DNA network structure. The above results sufficiently confirmed the feasibility of the DNA amplification strategy.

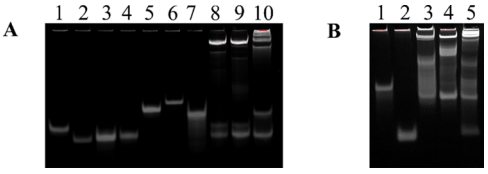

Figure 4. (A) PAGE analysis of DNFs: lane 1∼lane 4, A1∼A4; lane 5, P1; lane 6, P2; lane 7, TK1 mRNA; lane 8, DNF 1; lane 9, DNF 2; lane 10, DNF 1 + DNF 2 + TK1 mRNA. (B) PAGE characteristic of the 3D DNA network structure: lane 1, TK1 mRNA; lane 2, S0; lane 3, DNF 1; lane 4, DNF 2; lane 5, S0 + TK1 mRNA + DNF 1 + DNF 2.

Electrochemical Behaviors of the ECL Biosensor. The stepwise construction of the ECL biosensor was characterized by cyclic voltammetry (CV). As portrayed in Figure 5, the BCN NSs-Ru/Pt NPs/Nafion-coated GCE (curve b)

https://doi.org/10.1021/acs.analchem.2c02110
Anal. Chem. 2022, 94, 11345−11351

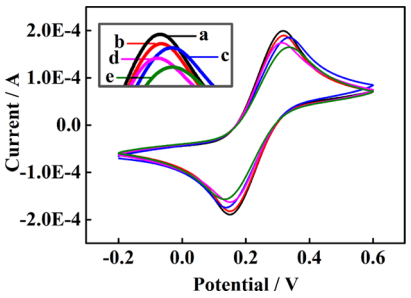

Figure 5. CV curves of the modificatory electrodes: (a) bare GCE, (b) (BCN NSs-Ru/Pt NPs/Nafion)/GCE, (c) S0/(BCN NSs-Ru/Pt NPs/Nafion)/GCE, (d) HT/S0/(BCN NSs-Ru/Pt NPs/Nafion)/GCE, and (e) 3D DNA network structure/HT/S0/(BCN NSs-Ru/Pt NPs/Nafion)/GCE.

presented a significantly weakened redox peak of $[Fe(CN)_6]^{3-/4-}$ due to its poor conductivity of Nafion compared with the bare GCE (curve a). When the modified GCE was sequentially decorated with S0 (curve c) and HT (curve d), the peak currents declined in turn on account of the formation of a DNA monolayer with negative charge and the immobilization of HT that blocked electron transfer. After that, with the import of the mixture of DNF 1, DNF 2, and target TK1 mRNA, the significantly decreased peak current was obtained (curve e), confirming that the target-induced DNA network labeled with multitudinous ferrocene was formed via the hybridization chain reaction of DNF 1 and DNF 2 triggered by TK1 mRNA to increase steric hindrance.

Stability, Reproducibility, and Selectivity of the Constructed Biosensor. Stability, reproducibility, and selectivity were evaluated to further investigate the properties of the prepared biosensor. The stability of our proposed biosensor was studied under consecutive cyclic potential scan to detect TK1 mRNA (100 fM and 10 pM), and the calculated relative standard deviation (RSD) values are shown in Figure 6A,B, which demonstrated the wonderful stability of our developed biosensor. Additionally, the relevant intra-assay and inter-assay experiments were carried out to assess the reproducibility of the biosensor. As shown in Figure 6C, the RSD values of intra-assay and inter-assay were 1.88 and 2.77%, respectively, suggesting that our designed biosensor had acceptable reproducibility. Moreover, four different biomolecules, including 1 nM one-base mismatched mRNA (TK1-M1), 1 nM double-base mismatched mRNA (TK1-M2), 1 nM tri-base mismatched mRNA (TK1-M3), and 1 nM irrelevant survivin mRNA (survivin), were treated as interference substances to further check out the selectivity of the biosensor. The proposed biosensor possessed a similar ECL response of the target TK1 mRNA (10 pM) and the mixture (containing 10 pM TK1 mRNA, 1 nM TK1-M1, 1 nM TK1-M2, 1 nM TK1-M3, and 1 nM survivin mRNA), while TK1-M1, TK1-M2, TK1-M3, and survivin mRNA showed no obvious difference compared to the blank group (Figure 6D), verifying the good selectivity of the fabricated biosensor. Therefore, the above results demonstrated that the TK1 mRNA biosensor showed fantastic stability, reproducibility, and selectivity.

Detection of TK1 mRNA Using the Designed Biosensor. Under the optimal conditions, the ECL biosensor was devoted to detecting a series of TK1 mRNA at increased concentrations. As illustrated in Figure 7, with the incremental concentration of TK1 mRNA changing from 100 aM to 100 nM, the corresponding ECL intensity gradually weakened. The ECL intensity discrepancy in comparison with that of the blank group (ΔI) and the lg c (TK1 mRNA) showed an outstanding linear relationship, which fitted as the regression equation $\Delta I = 4090.58 + 1543.92 \lg c$ ($R^2 = 0.9965$) with a detection limit of 32.3 aM, revealing better analytical performance than that reported in previous studies (Table 1).

Performance of the Obtained Biosensor in MCF-7 Cell Analysis. To verify practicability of the obtained biosensor, human breast cancer cell (MCF-7) extract with

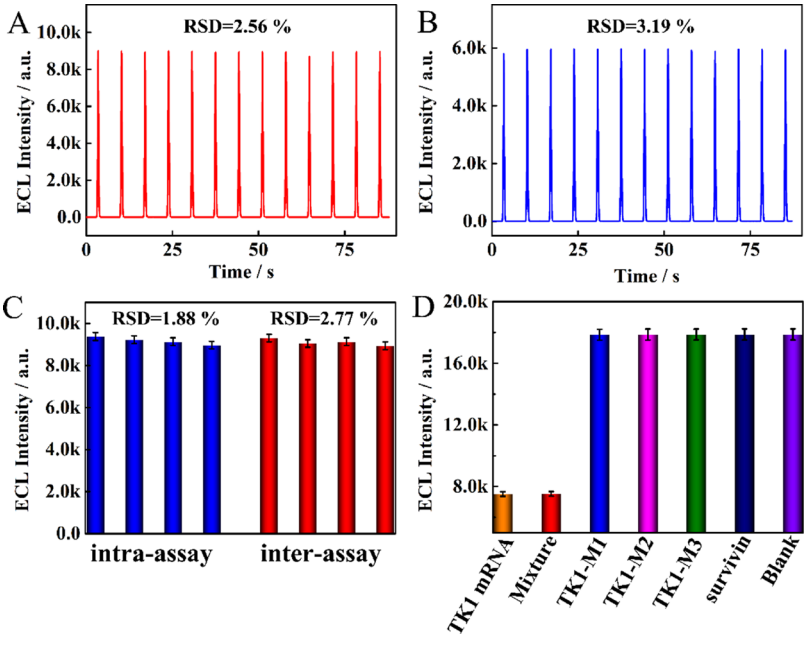

Figure 6. Stability study of this biosensor incubated toward 100 aM (A) and 1 nM (B) TK1 mRNA at the continuous cyclic of potential scanning; reproducibility of the designed strategy (C); selectivity of the TK1 mRNA biosensor with four different distractors (D). Error bars appearing throughout the manuscript represent standard deviations of three repeated experiments.

https://doi.org/10.1021/acs.analchem.2c02110
Anal. Chem. 2022, 94, 11345−11351

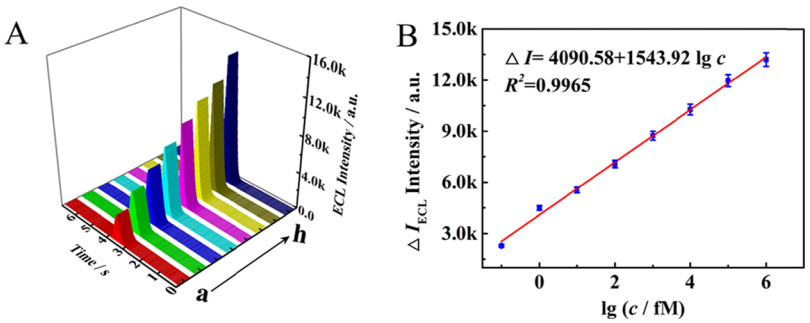

Figure 7. ECL signal of the constructed biosensor with different TK1 mRNA concentrations (A): (a) 1 nM, (b) 100 pM, (c) 10.0 pM, (d) 1 pM, (e) 100 fM, (f) 10.0 fM, (g) 1 fM, and (h) 100 aM. Calibration curve for TK1 mRNA determination (B).

Table 1. Comparison of Different RNA Detection Methods

analytical method	detection limit	dynamic range	references
FL	20 fM	50 fM to 500 pM	38
Raman	2.33 fM	10 fM to 10 nM	39
chemiluminescence	0.3 pM	10 pM to 100 nM	40
ECL	0.13 fM	1 fM to 1 nM	41
ECL	0.331 fM	1 fM to 10 nM	42
ECL	32.3 aM	100 aM to 1 nM	this work

cell concentrations from 10^0 to 10^5, obtained by treating a known number of cells with an RNA extraction kit, was applied to record the ECL intensity of the biosensor. In Figure 8A, a series of ECL signals decreased with the increase of the cell number. Additionally, the ECL intensity diminution (ΔI_{ECL}) meets the regression equation $\Delta I = 4825.24 + 1507.17 \lg N$ ($R^2 = 0.9972$, Figure 8B). Hence, the result demonstrated that our developed biosensor possessed good potential in practical detection.

CONCLUSIONS

In short, based on a unique self-enhanced nanocomposite BCN NSs-Ru with high ECL efficiency as an emitter, we have constructed an ultrasensitive biosensor to detect the target TK1 mRNA in the acid of target-induced 3D DNA network structure. First, BCN NSs possessed outstanding chemical stability, excellent adsorption performance, and catalytic oxygen reduction reaction ability. Second, electron tunneling between ultrathin BCN NS layers could achieve faster electron transfer, which was conducive to fast and efficient intramolecular reactions. Third, the amine groups and unsaturated boron atoms at the edges or defects of BCN NSs were the sources of active radicals, which could be used to obviously improve ECL efficiency of $Ru(dcbpy)_3^{2+}$. Therefore, the strategy offered a new means for biomolecular detection and disease diagnosis.

ASSOCIATED CONTENT

Supporting Information

The Supporting Information is available free of charge at https://pubs.acs.org/doi/10.1021/acs.analchem.2c02110.

Experimental details for reagents and apparatus, preparation of BCN NSs, the synthesis of BCN NSs-Ru, preparation of Pt nanoparticles, preparation of ferrocene-labeled DNA nanoflowers, optimization of the experimental conditions, characterization of Pt NPs, AFM characterization of the BCN NSs, TEM and AFM characterization of DNFs, UV−vis absorption spectroscopy of the nanomaterials, research with the self-enhancement of BCN NSs-Ru, exploration of the quenching effect of the 3D network structure with ferrocene, and the calculation of the limit of detection (PDF)

AUTHOR INFORMATION

Corresponding Authors

Yaqin Chai − *Key Laboratory of Luminescence Analysis and Molecular Sensing (Southwest University), Ministry of Education, College of Chemistry and Chemical Engineering, Southwest University, Chongqing 400715, PR China;* orcid.org/0000-0003-4392-9592; Email: yqchai@swu.edu.cn

Ruo Yuan − *Key Laboratory of Luminescence Analysis and Molecular Sensing (Southwest University), Ministry of Education, College of Chemistry and Chemical Engineering, Southwest University, Chongqing 400715, PR China;*

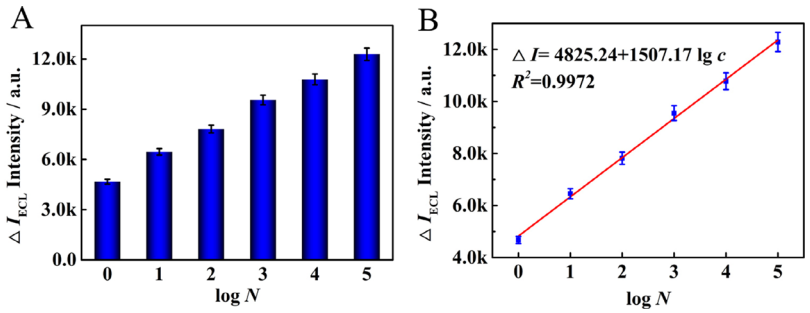

Figure 8. Detection signal of TK1 mRNA in the lysate of MCF-7 cells at the cell concentrations from 10^0 to 10^5 using our fabricated biosensor (A). Calibration plot for TK1 mRNA determination in MCF-7 cell lysates (B).

https://doi.org/10.1021/acs.analchem.2c02110
Anal. Chem. 2022, 94, 11345−11351

orcid.org/0000-0003-3664-6236; Email: yuanruo@swu.edu.cn

Authors

Jicui Hu − *Key Laboratory of Luminescence Analysis and Molecular Sensing (Southwest University), Ministry of Education, College of Chemistry and Chemical Engineering, Southwest University, Chongqing 400715, PR China*

Yue Zhang − *Key Laboratory of Luminescence Analysis and Molecular Sensing (Southwest University), Ministry of Education, College of Chemistry and Chemical Engineering, Southwest University, Chongqing 400715, PR China*

Complete contact information is available at: https://pubs.acs.org/10.1021/acs.analchem.2c02110

Notes

The authors declare no competing financial interest.

■ ACKNOWLEDGMENTS

The authors thank the National Natural Science Foundation of China (Grant Nos. 22174113, 22176153, and 21974108).

■ REFERENCES

(1) Li, J.; Jia, H.; Ren, X.; Li, Y.; Liu, L.; Feng, R.; Ma, H.; Wei, Q. *Small* **2022**, *18*, 1−11.
(2) Xiao, S.; Wang, X.; Yang, C.; Jiang, Y.; Zhen, S.; Huang, C.; Li, Y. *Anal. Chem.* **2022**, *94*, 1178−1186.
(3) Wang, X.; Wang, X.; Hu, C.; Guo, W.; Wu, X.; Chen, G.; Dai, W.; Zhen, S.; Huang, C.; Li, Y. *Biosens. Bioelectron.* **2022**, *213*, No. 114443.
(4) Li, Y. X.; Li, J.; Cai, W. R.; Xin, W. L.; Marks, R. S.; Zeng, H. B.; Cosnier, S.; Zhang, X.; Shan, D. *Anal. Chem.* **2020**, *92*, 15270−15274.
(5) Wang, Y.; Zhao, G.; Chi, H.; Yang, S.; Niu, Q.; Wu, D.; Cao, W.; Li, T.; Ma, H.; Wei, Q. *J. Am. Chem. Soc.* **2021**, *143*, 504−512.
(6) Wang, Y.; Guo, W.; Yang, Q.; Su, B. *J. Am. Chem. Soc.* **2020**, *142*, 1222−1226.
(7) Liu, Y.; Zhang, H.; Li, B.; Liu, J.; Jiang, D.; Liu, B.; Sojic, N. *J. Am. Chem. Soc.* **2021**, *143*, 17910−17914.
(8) Ding, H.; Zhou, P.; Fu, W.; Ding, L.; Guo, W.; Su, B. *Angew. Chem., Int. Ed.* **2021**, *60*, 11769−11773.
(9) Liu, S.; Yuan, H.; Bai, H.; Zhang, P.; Lv, F.; Liu, L.; Dai, Z.; Bao, J.; Wang, S. *J. Am. Chem. Soc.* **2018**, *140*, 2284−2291.
(10) Han, D.; Goudeau, B.; Manojlovic, D.; Jiang, D.; Fang, D.; Sojic, N. *Angew. Chem., Int. Ed.* **2021**, *60*, 7686−7690.
(11) Ma, Y.; Colin, C.; Descamps, J.; Arbault, S.; Sojic, N. *Angew. Chem., Int. Ed.* **2021**, *60*, 18742−18749.
(12) Huang, W.; Hu, G. B.; Yao, L. Y.; Yang, Y.; Liang, W. B.; Yuan, R.; Xiao, D. R. *Anal. Chem.* **2020**, *92*, 3380−3387.
(13) Ye, J.; Liu, G.; Yan, M.; Zhu, Q.; Zhu, L.; Huang, J.; Yang, X. *Anal. Chem.* **2019**, *91*, 13237−13243.
(14) Zhuo, Y.; Liao, N.; Chai, Y. Q.; Gui, G. F.; Zhao, M.; Han, J.; Xiang, Y.; Yuan, R. *Anal. Chem.* **2014**, *86*, 1053−1060.
(15) Wang, J.; Hao, J.; Liu, D.; Qin, S.; Portehault, D.; Li, Y.; Chen, Y.; Lei, W. *ACS Energy Lett.* **2017**, *2*, 306−312.
(16) Peng, D.; Jiang, W.; Li, F. F.; Zhang, L.; Liang, R. P.; Qiu, J. D. *ACS Sustainable Chem. Eng.* **2018**, *6*, 11685−11694.
(17) Sun, M. F.; Liu, J. L.; Zhou, Y.; Zhang, J. Q.; Chai, Y. Q.; Li, Z. H.; Yuan, R. *Anal. Chem.* **2020**, *92*, 14723−14729.
(18) Liu, Z.; Liu, J.; Mateti, S.; Zhang, C.; Zhang, Y.; Chen, L.; Wang, J.; Wang, H.; Doeven, E. H.; Francis, P. S.; Barrow, C. J.; Du, A.; Chen, Y.; Yang, W. *ACS Nano* **2019**, *13*, 1394−1402.
(19) Carrara, S.; Arcudi, F.; Prato, M.; De Cola, L. *Angew. Chem., Int. Ed.* **2017**, *56*, 4757−4761.
(20) Cheng, H.; Liu, J.; Ma, W.; Duan, S.; Huang, J.; He, X.; Wang, K. *Anal. Chem.* **2018**, *90*, 12544−12552.
(21) Gao, R.; Hao, C.; Xu, L.; Xu, C.; Kuang, H. *Anal. Chem.* **2018**, *90*, 5414−5421.
(22) Shi, J.; Zhou, M.; Gong, A.; Li, Q.; Wu, Q.; Cheng, G. J.; Yang, M.; Sun, Y. *Anal. Chem.* **2016**, *88*, 1979−1983.
(23) Kim, Y. J.; Nomakuchi, T.; Papaleonidopoulou, F.; Yang, L.; Zhang, Q.; Krainer, A. R. *Nat. Commun.* **2022**, *13*, 2978.
(24) Metelev, M.; Lundin, E.; Volkov, I. L.; Gynnå, A. H.; Elf, J.; Johansson, M. *Nat. Commun.* **2022**, *13*, 1−13.
(25) Zhao, X.; Ji, X.; Qu, J.; Xie, K.; Wang, Z.; Fang, P.; Wang, Y.; Wan, Y.; Yang, Y.; Zhang, W.; Shi, P. *J. Am. Chem. Soc.* **2022**, *144*, 6010−6018.
(26) He, M.; He, M.; Nie, C.; Yi, J.; Zhang, J.; Chen, T.; Chu, X. *ACS Appl. Mater. Interfaces* **2021**, *13*, 8015−8025.
(27) Lin, Q.; Ye, X.; Huang, Z.; Yang, B.; Fang, X.; Chen, H.; Kong, J. *Anal. Chem.* **2019**, *91*, 15694−15702.
(28) Yu, S.; Zhou, Y.; Sun, Y.; Wu, S.; Xu, T.; Chang, Y. C.; Bi, S.; Jiang, L. P.; Zhu, J. J. *Angew. Chem., Int. Ed.* **2021**, *60*, 5948−5958.
(29) Ding, Q.; Zhan, Q.; Zhou, X.; Zhang, T.; Xing, D. *Small* **2016**, *12*, 5944−5953.
(30) Wang, D. X.; Wang, J.; Cui, Y. X.; Wang, Y. X.; Tang, A. N.; Kong, D. M. *Anal. Chem.* **2019**, *91*, 13165−13173.
(31) Li, Z.; Yang, H.; Hu, M.; Zhang, L.; Ge, S.; Cui, K.; Yu, J. *ACS Appl. Mater. Interfaces* **2020**, *12*, 17177−17184.
(32) Wang, J.; Wang, D. X.; Ma, J. Y.; Wang, Y. X.; Kong, D. M. *Chem. Sci.* **2019**, *10*, 9758−9767.
(33) Wang, T.; Peng, Q.; Guo, B.; Zhang, D.; Zhao, M.; Que, H.; Wu, H.; Yan, Y. *Biosens. Bioelectron.* **2020**, *150*, No. 111954.
(34) Yang, F.; Jiang, X. Y.; Liang, W. B.; Chai, Y. Q.; Yuan, R.; Zhuo, Y. *Anal. Chem.* **2020**, *92*, 2566−2572.
(35) Dong, Y.; Yao, C.; Zhu, Y.; Yang, L.; Luo, D.; Yang, D. *Chem. Rev.* **2020**, *120*, 9420−9481.
(36) Wu, F. F.; Zhou, Y.; Zhang, H.; Yuan, R.; Chai, Y. Q. *Anal. Chem.* **2018**, *90*, 2263−2270.
(37) Jin, Z.; Zhu, X.; Wang, N.; Li, Y.; Ju, H.; Lei, J. *Angew. Chem., Int. Ed.* **2020**, *59*, 10446−10450.
(38) Zhang, H.; Huang, X.; Liu, J.; Liu, B. *Chem. Sci.* **2020**, *11*, 3812−3819.
(39) Wang, Z.; Ye, S.; Zhang, N.; Liu, X.; Wang, M. *Anal. Chem.* **2019**, *91*, 5043−5050.
(40) Sun, Y.; Shi, L.; Wang, Q.; Mi, L.; Li, T. *Anal. Chem.* **2019**, *91*, 3652−3658.
(41) Hao, Q.; Xu, Q.; Niu, S.; Ding, C.; Luo, X. *Anal. Chem.* **2021**, *93*, 10679−10687.
(42) Wang, Q.; Liu, Y.; Yan, J.; Liu, Y.; Gao, C.; Ge, S.; Yu, J. *Anal. Chem.* **2021**, *93*, 13373−13381.